Impact of local structure on melt dynamics in Cu-Ti alloys: Insights from *ab initio* molecular dynamics simulations

Lucas P. Kreuzer [1,2,*] Fan Yang [2] Andreas Meyer [2,3] and Noël Jakse [4]

[1] *Heinz Maier-Leibnitz-Zentrum, Technische Universität München, Lichtenbergstraße 1, 85748 Garching, Germany*

[2] *Institut für Materialphysik im Weltraum, Deutsches Zentrum für Luft- und Raumfahrt (DLR), 51170 Köln, Germany*

[3] *Institut Laue-Langevin (ILL), 71 avenue des Martyrs, 38042 Grenoble, France*

[4] *Université Grenoble Alpes, CNRS, Grenoble INP, SIMaP, F-38000 Grenoble, France*

(Received 1 December 2024; revised 27 February 2025; accepted 28 March 2025; published 23 April 2025)

First-principles based molecular-dynamics simulations have been performed for binary Cu_xTi_{1-x} ($x = 0.31$, 0.50, and 0.76) alloys to investigate the relationship between local structure and dynamical properties in the liquid and undercooled melt. The undercooled melts show a pronounced short-range order, majorly a fivefold symmetry (FFS) around the Cu atoms, which competes with bcc ordering. This complex SRO is also reflected in the partial coordination numbers, where mainly a Z12 coordination is present around Cu, which corresponds to an icosahedral ordering. Higher coordination numbers were obtained for Ti compatible with Frank-Kasper polyhedra. The increasing Frank-Kasper polyhedra coordination scenario around Ti impacts the interatomic distances of Ti atoms, which increase with increasing Ti content. The $Cu_{50}Ti_{50}$ composition exhibits the highest FFS ordering and amount of Frank-Kasper polyhedra, which explains the slowest melt dynamics, found experimentally and in simulations for this composition. Thus, our results suggest that the high undercooling degree originates from the high complexity of the local structure rather than due to the preferred formation of Cu-Ti pairs, as Cu-Ti interactions were found to be weak.

DOI: 10.1103/PhysRevB.111.144107

I. INTRODUCTION

Bulk metallic glasses feature an amorphous structure in their solid state, which gives them superior mechanical properties compared to their crystalline counterparts. Besides complex multicomponent alloy systems, relatively simple binary systems are also known to show excellent glass-forming abilities (GFA) [1–5]. Even for binary systems, the underlying mechanisms responsible for a good GFA are still not fully understood on atomic length and timescales [6–10]. Using them as model systems to understand structural and dynamical properties, especially in the undercooled region, where nucleation and growth [11] or glass formation [12] take place, is of utmost importance.

Among the most well-known and widely studied binary glass-forming alloys are Zr-based systems, e.g., Cu-Zr and Ni-Zr. Over the last years, numerous experimental and computational studies were reported on the relationship between structure and dynamics in the melt to explain the observed high GFA [2,13–16]. Zr-Cu alloys exhibit better GFAs compared to Zr-Ni alloys [1,2]. However, the atomic dynamics of Zr-Ni melts are slower than that in the Zr-Cu melts [15,17]. This is surprising, since sluggish dynamics usually promote glass formation [18]. A higher nucleation barrier for the Zr-Cu system due to a pronounced icosahedral and chemical short-range order (SRO), especially on the Cu-rich side of the phase diagram, might be an explanation [14], which demonstrates the close relation between the SRO and the properties of the melt.

For understanding the melt dynamics, it has been found that the composition-dependent dynamics in Zr-Cu can be understood by the packing density, i.e., a more densely packed melt results in slower melt dynamics [15]. When replacing Cu with Ni, which has a similar atomic radius, the melt dynamics become slower, which cannot be explained by a change of geometric packing in the liquid only [19]. Similarly, when substituting Zr by Hf (both are chemically similar, as they have approximately the same atomic radius and are located in the same main group of the periodic table), the melt dynamics also become slower, which is attributed to a locally higher packing density as a result of preferred formation of Hf-Ni nearest-neighbor pairs [20]. Furthermore, for Zr-Ni melts, a decoupling of the Ni diffusivity from the Zr diffusivity can be observed in the Ni-rich compositions, which can be attributed to the saturation of chemical interactions between Zr and Ni. Thus, besides packing and dynamical arguments, chemical interactions also seem to play a crucial role for the structure-dynamics relationship in the melt.

Substitution of Zr by Ti, which stands above Zr in the fourth element group, underlines this presumption. In a recent study by us, we found a mixing behavior of the molar volume close to an ideal solution, resulting in an almost

*Contact author: lucas.kreuzer@frm2.tum.de

constant packing fraction for the binary Cu-Ti system [21]. The obtained values of the packing fraction are similar to that of the Cu-Zr system, but slightly lower than that of the Ni-Zr system [15,17]. The melt viscosity of Cu-Ti features a nonmonotonous trend with increasing Ti concentration and exhibits the largest values around an intermediate Ti concentration of 50 at.%. The slowdown of the dynamics refers to chemical interactions between Cu and Ti, which form preferred neighboring pairs. Indeed, a chemical SRO was found, however, it is less pronounced as, e.g., for Ni-Zr and Ni-Hf, which might explain the overall faster atomic dynamics in the Cu-Ti system as compared to the above-mentioned Ni-based alloys [17,20]. These differences in average packing fraction and liquid viscosity clearly point to composition- and concentration-dependent interactions between the alloy components within these systems.

Especially, the large differences between the Cu-Zr and Cu-Ti systems, regarding the structure-dynamics relationship, despite a similar electronic configuration and atomic radius ($r_{Zr} = 1.450$ Å; $r_{Ti} = 1.324$ Å), cannot be explained yet. Hence, information about how chemical interactions control the liquid dynamics over a broad temperature range and as a function of composition are needed, e.g., by accessing partial structure factors, particularly $S_{CC}(q)$. However, measuring partial structure factors is challenging, and so far only the $S_{CC}(q)$ for $Cu_{31}Ti_{69}$ at 1000 K has been obtained experimentally [21]. An elegant solution to this is the use of simulations, validated on the existing experimental data of the Cu-Ti system, and provide access to structure and dynamics over a broad composition range. Thereby, the role of chemical interactions for the liquid dynamics can be resolved, which contributes to an understanding of how the structure-dynamics relationship is (or is not) correlated with the GFA, and if such a relationship is universal for other (binary) alloys as well. Besides a fundamental interest, answering these questions is also of relevance for industrial processes. Ti is cheaper and lighter than Zr, which would enable new application fields, especially in the lightweight sector, e.g., as alloys for aerospace or automotive applications.

The present paper aims at resolving the structure-dynamics relationship and shedding light on recent experimental studies on the Cu-Ti system. *Ab initio* molecular dynamics (AIMD) simulations within the density functional theory (DFT) were performed to elucidate the structural and dynamic properties of liquid and undercooled Cu-Ti alloys [22–26]. A compositional range spanning from 24 to 69 at.% Ti, specifically targeting the compositions of $Cu_{76}Ti_{24}$, $Cu_{50}Ti_{50}$, and $Cu_{31}Ti_{69}$, which were also investigated experimentally, across a broad temperature range from 1000 to 1700 K, also including former results from pure Cu and Ti. The simulations provide detailed insights into the local structure, partial interatomic particle distances, coordination number, composition-dependent diffusion coefficients, and present symmetries in the melt and undercooled liquid, which are not experimentally accessible but needed for a fully comprehensive understanding of the structure-dynamics relationship.

In this paper, a pronounced fivefold symmetry (FFS) in the undercooled melt is observed, particularly around Cu atoms, competing with a bcc ordering. A Z12 coordination is present around Cu, and higher coordinated Frank-Kasper polyhedra around Ti. The FFS and Frank-Kasper coordination is found to be the highest for the equiatomic $Cu_{50}Ti_{50}$ composition, which gives an explanation for the experimentally found viscosity maximum for this composition.

TABLE I. Number of atoms of each species for all liquid Cu-Ti alloys used in the corresponding VASP simulations. The total number of atoms is $N = 256$.

	$Cu_{31}Ti_{69}$		Cu_{50} Ti_{50}		$Cu_{76}Ti_{24}$	
	Cu	Ti	Cu	Ti	Cu	Ti
Number of atoms	79	177	128	128	195	61
Box size (1000 K)	16.174 Å		15.845 Å		15.331 Å	
Box size (1100 K)	16.211 Å		15.888 Å		15.390 Å	
Box size (1200 K)	16.248 Å		15.932 Å		15.450 Å	
Box size (1300 K)	16.287 Å		15.985 Å		15.510 Å	
Box size (1400 K)	16.329 Å		16.031 Å		15.559 Å	
Box size (1500 K)	16.363 Å		16.067 Å		15.634 Å	
Box size (1600 K)	16.401 Å		16.112 Å		15.697 Å	
Box size (1700 K)	16.441 Å		16.159 Å		15.761 Å	

II. COMPUTATIONAL BACKGROUND

The structural and dynamic characteristics of binary $Cu_{76}Ti_{24}$, $Cu_{50}Ti_{50}$, and $Cu_{31}Ti_{69}$ liquid alloys within a temperature range of 1000 to 1700 K were investigated using AIMD simulations within the framework of the DFT, employing the VIENNA AB INITIO SIMULATION PACKAGE (VASP) [27]. The electron-ion interaction was represented by the project augmented wave potentials [28,29]. For exchange and correlation effects, the generalized gradient approximation in the Perdew, Burke, and Ernzerhof formulation was applied [30]. The cutoff energy in plane-wave expansion was taken as the default one for Cu, namely, 295 eV. For such large supercells in the liquid state, only the Γ_0 point was used for sampling the Brillouin zone. Phase space trajectories were generated through dynamical simulations by numerical integration of Newton's equations of motion using the standard Verlet algorithm in the velocity form, with a time step of 1.5 fs. All simulations were conducted within cubic boxes containing $N = 256$ atoms, with periodic boundary conditions applied in all spatial directions. The number of atoms for each species in the simulations is listed in Table I. The volume V of each simulation was adjusted to match experimentally determined densities. An analysis of the pressure tensor ensured that the pressure remained within an acceptable range of GPa, which is of the order of the pressure fluctuations. The respective simulation box sizes are listed in Table I as well. Temperature control was achieved using a Nosé thermostat within the canonical ensemble (constant N, V, and T) [31], with thermalization performed for a minimum of 20 ps, guided by the relaxation time determined from the self-intermediate scattering functions $F_S(q,t)$ [32]. Structural and dynamic properties were extracted from simulations spanning from 12 to 40 ps for each temperature. The shear viscosity was calculated from the diffusion coefficient using the Stokes-Einstein relation. Equilibrated trajectories at each temperature were

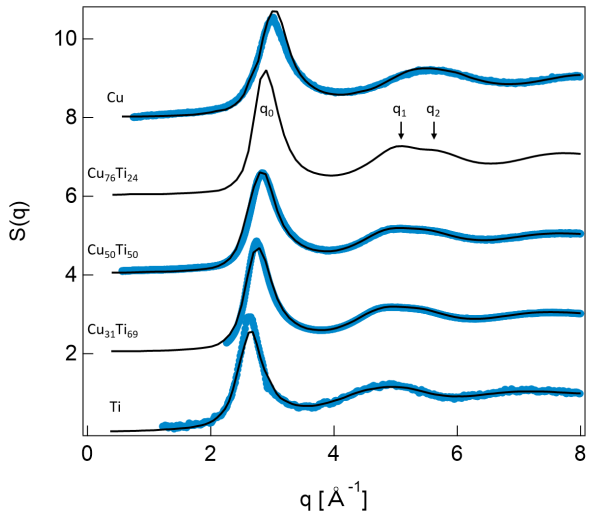

FIG. 1. AIMD calculations (black lines) of the total x-ray structure factor $S(q)$ in liquid Cu_xTi_{1-x} (from bottom to top: $x = 0$, 0.31, 0.50, 0.76, 1). Experimental data (blue points) are shown for comparison. The binary alloys have been measured at 1273 K [21], while the pure Cu and Ti have been measured at 1398 K and 1848 K, respectively [36,37]. The AIMD have been performed at similar temperatures (1300 K for the binary alloys and 1398 K and 1848 K for pure Cu and Ti, respectively).

sampled regularly to obtain ten configurations and then relax the inherent structure [33]. This step is crucial for decoupling vibrational motion from underlying structural properties by minimizing the potential-energy surface of the atoms, thereby reducing noise in the common neighbor analysis (CNA) index calculations. Structural analysis was conducted using the CNA method, implemented through various Python modules of the Open Visualization Tool (OVITO) [34,35].

III. RESULTS AND DISCUSSION

A. Structural properties

The reliability of the performed AIMD simulations is verified by comparison with already existing experimental data. Figure 1 shows the total structure factor $S(q)$ for the binary $Cu_{76}Ti_{24}$, $Cu_{50}Ti_{50}$, and $Cu_{31}Ti_{69}$ liquid alloys as well as for pure liquid Cu and Ti, obtained from experiments and AIMD. The experimental data were obtained using x-ray diffraction and electrostatic levitation [21]. For $S(q)$ of the Cu-rich $Cu_{76}Ti_{24}$ composition, only simulation results are available. The binary alloys were measured at 1273 K, the pure Cu and Ti at 1398 K and 1848 K, respectively. The AIMD were performed at similar temperatures (1300 K for the binary alloys and 1398 K and 1848 K for pure Cu and Ti, respectively). Both, AIMD and experimental data agree very well regarding the position and amplitude of the first peak and the subsequent oscillations. Generally, this is a first indication of the reliability of the performed simulations.

For all three investigated Cu-Ti compositions, a shoulder at the second peak of the structure factor $S(q)$ is observed. Especially for $Cu_{76}Ti_{24}$, this shoulder is strongly pronounced. This feature in the scattering data suggests a preferred icosahedral SRO (ISRO) in the melt. Within the Ginzburg-Landau theory to describe the ISRO in undercooled liquids and metallic glasses [38], it can be further investigated by calculating the ratio of the position of the first and second peak maxima q_0 and q_2 as well as the respective shoulder q_1 (as is also shown in Fig. 1). For a perfect ISRO, values of $q_1/q_0 \approx 1.7$ and $q_2/q_0 \approx 2$ are expected, whereas the calculated values for the respective compositions are listed in Table II and are slightly larger (in the case of q_1/q_0) or lower (q_2/q_0). Thus, a non-negligible fraction of ISRO is present within all three investigated Cu-Ti compositions, however, not a perfect one, as is expected for a binary alloy with atoms of different sizes.

TABLE II. Ratio of q_1/q_0 and q_2/q_0 for all Cu-Ti compositions under investigation.

	$Cu_{31}Ti_{69}$	$Cu_{50}Ti_{50}$	$Cu_{76}Ti_{24}$
q_1/q_0	1.79	1.78	1.77
q_2/q_0	1.91	1.84	1.90

Furthermore, AIMD calculations of the partial concentration-concentration structure factor $S_{CC}(q)$ and pair-correlation function $g_{CC}(r)$ are compared with experimental results that have been obtained by neutron diffraction (again in combination with electrostatic levitation) in Fig. 2. $S_{CC}(q)$ quantifies the spatial correlations of compositional fluctuations, and its Fourier transform represents the distribution of the chemical species. Thus, $S_{CC}(q)$ gives an idea of the chemical order of the described Cu-Ti melts. The simulated $S_{CC}(q)$ and $g_{CC}(r)$ exhibit qualitative agreement with the experimental data, while some differences are observed. Nevertheless, the congruence is remarkable, since $S_{CC}(q)$ reflects on the chemical interactions, which are very challenging to integrate into computational models. The good overlap of experimental data and simulation, as in previous work, shows that the AIMD framework used cannot only reproduce the

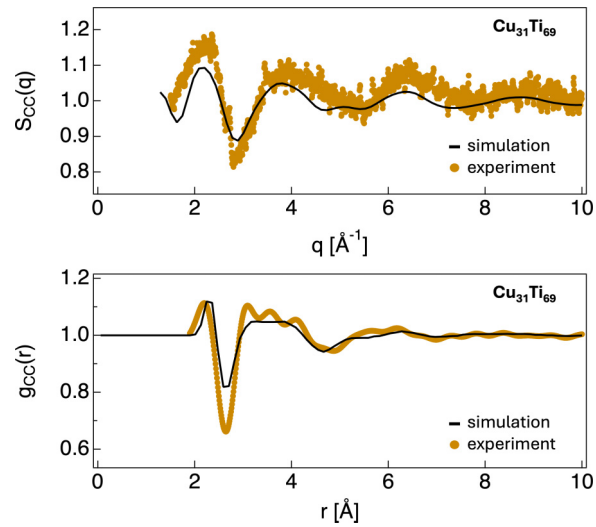

FIG. 2. Simulated (black lines) concentration-concentration structure factor $S_{CC}(q)$ (top) and pair-correlation function $g_{CC}(r)$ (bottom) of $Cu_{31}Ti_{69}$ at 1300 K. Experimental data (orange points) of $S_{CC}(q)$ and $g_{CC}(r)$ of $Cu_{31}Ti_{69}$ from neutron diffraction experiments ($T = 1273$ K) are shown for comparison [21].

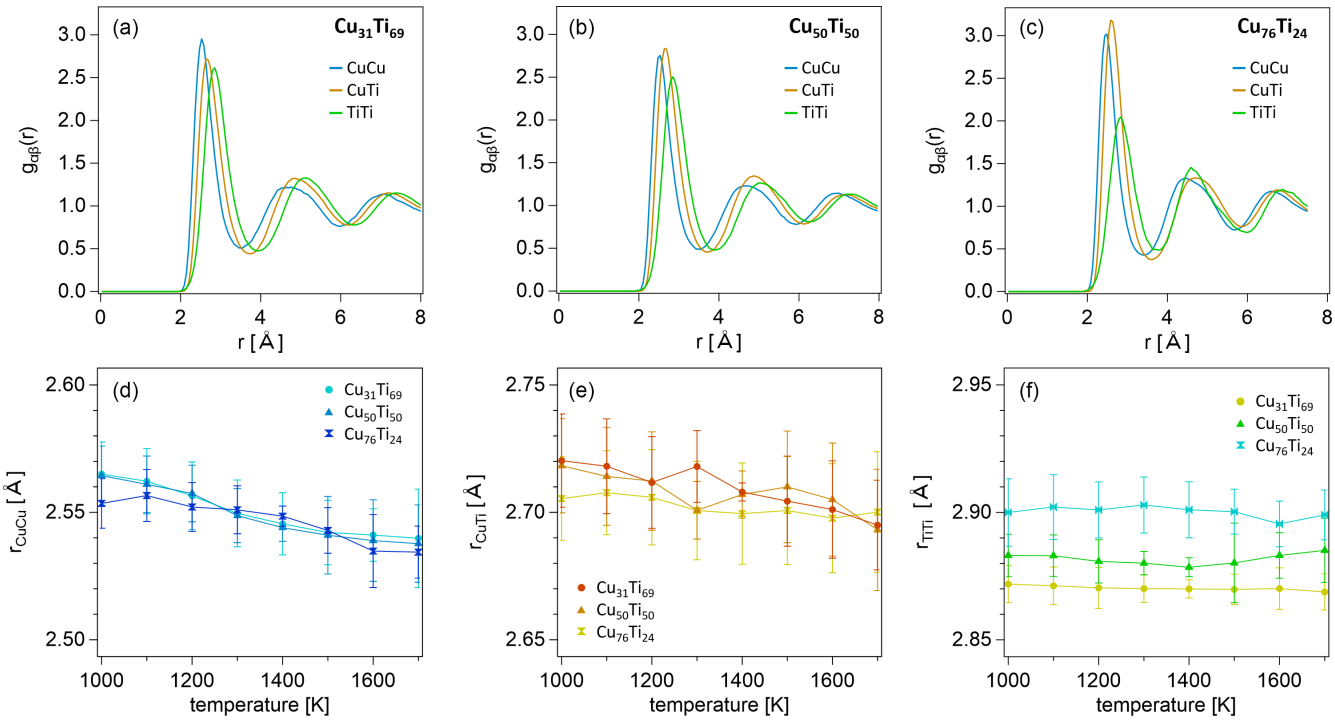

FIG. 3. Partial pair-correlation functions of (a) $Cu_{31}Ti_{69}$, (b) $Cu_{50}Ti_{50}$, and (c) $Cu_{76}Ti_{24}$ at a temperature of 1300 K. In the bottom row, the positions of the first maxima of $r_{\alpha\beta}$, which represent the interatomic particle distance between (d) CuCu, (e) CuTi, and (f) TiTi, respectively, are shown as a function of temperature.

general structural and dynamic properties but also correctly accounts for chemical interactions present within the Cu-Ti system [24,25,39].

In the following, the structural properties, i.e., local structures, coordination numbers, and symmetries of Cu-Ti melts from AIMD are discussed. Subsequently, the melt dynamics through the mean self-diffusion coefficient and shear viscosity as well as the correlation of the dynamic properties with the local melt structure will be analyzed.

Partial pair-correlation functions $g_{\alpha\beta}(r)$ obtained from the AIMD simulations are shown in Figs. 3(a)–3(c) at an exemplary temperature of 1300 K for the three investigated compositions. Figures 3(d)–3(f) plot the first peak maxima position $r_{\alpha\beta}(T)$ of the respective $g_{\alpha\beta}(r)$ as a function of temperature. $r_{\alpha\beta}(T)$ represents the average first-neighbor distance and thus the Cu-Cu, Cu-Ti, and Ti-Ti bond lengths, respectively. For all three compositions, we find the Cu-Cu distances to be shortest and Ti-Ti distances to be longest, which is due to the larger atomic radius of Ti ($r_{\mathrm{Ti}} = 1.324$ Å and $r_{\mathrm{Cu}} = 1.173$ Å). While the Cu-Cu and Cu-Ti distances feature no composition dependence, the average Ti-Ti distance [Fig. 3(f)] displays increasing distances upon increasing Cu concentration. The lowest and highest Ti-Ti distance is observed for the Ti-rich and Ti-poor $Cu_{31}Ti_{69}$ ($r_{\mathrm{TiTi}} \approx 2.87$ Å) and $Cu_{76}Ti_{24}$ ($r_{\mathrm{TiTi}} \approx 2.90$ Å) composition, respectively. This observation can be attributed to extraordinary high coordination numbers around Ti, in particular, for the $Cu_{76}Ti_{24}$ composition, as will be explained later. Figures 3(d)–3(e) highlights that with increasing temperature, the average distances display a small decrease, which is slightly more pronounced for Cu-Cu and Cu-Ti. Such a trend was also observed for pure elements and can be correlated with an increase in coordination number, as will be discussed later in the text [22]. The values for r_{TiTi} remain constant with temperature. To put these values into context, the atomic distances between Cu and Ti in the pure melts are slightly smaller as the respective distances in the alloys ($r_{\mathrm{CuCu,\,pure}} = 2.48$ Å and $r_{\mathrm{TiTi,\,pure}} = 2.80$ Å) [36,37,40]. The amplitudes of $g_{\alpha\beta}(r)$ relatively to each other change, showing an evolution from an ideal mixing at low Cu content to a more pronounced heterocoordination with increasing Cu composition, as revealed by the amplitude of g_{CuTi} which increases, whereas those of g_{TiTi} decrease. As a matter of fact, a monotonous decrease from the amplitude of $g_{\mathrm{CuCu}}(r)$ to $g_{\mathrm{CuTi}}(r)$ and $g_{\mathrm{TiTi}}(r)$ ($A_{g_{\mathrm{CuCu}}} > A_{g_{\mathrm{CuTi}}} > A_{g_{\mathrm{TiTi}}}$) is observed for $Cu_{31}Ti_{69}$ [see Fig. 3(a)] and typically corresponds to an ideal solution behavior [41]. The more pronounced $g_{\mathrm{CuTi}}(r)$ for the other two compositions $Cu_{50}Ti_{50}$ and $Cu_{76}Ti_{24}$ suggests a deviation from such an ideal solution behavior. In the literature, the solution behavior was studied experimentally and different results were obtained: Amore *et al.* observed a strong deviation from the ideal solution behavior, with a maximum at the Ti-rich side [42,43]. In contrast, some of us recently reported a solution behavior that is closer to the ideal case, with a maximal deviation found for intermediate Ti contents. One should note that no data for a Cu-rich alloy was shown there [21]. The different results on the solution behavior reported in Refs. [21,43] refer to different measurement and sample processing techniques, which also highlight the sensitivity and complexity of the Cu-Ti system. The results obtained from AIMD simulation feature better agreement with the experimental results from Ref. [21].

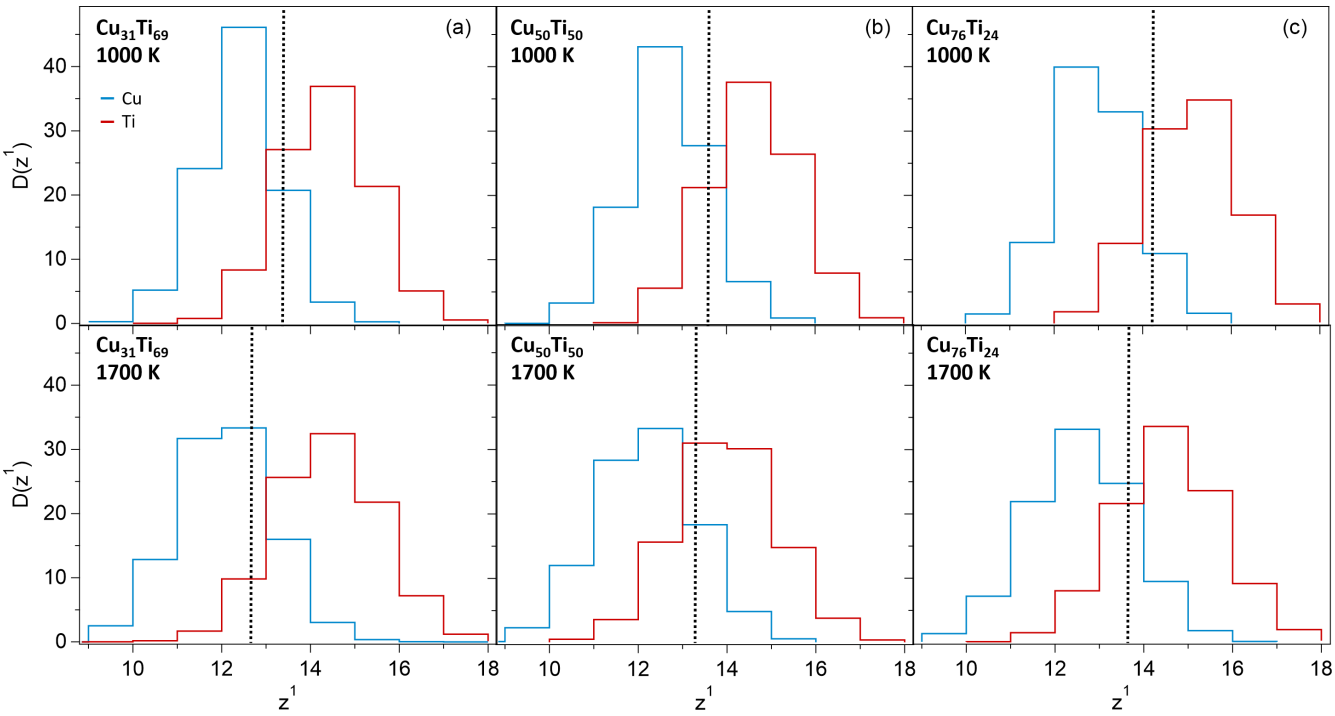

FIG. 4. Distribution of the coordination numbers z^1 for typical configurations of (a) $Cu_{31}Ti_{69}$, (b) $Cu_{50}Ti_{50}$, and (c) $Cu_{76}Ti_{24}$ in the deeply undercooled (1000 K, top row) and liquid state (1700 K, bottom row) for Cu (blue) and Ti (red). The vertical black dashed lines indicate the average coordination number for the respective Cu-Ti composition.

As already mentioned, with decreasing Ti-content, the Cu-Ti affinity becomes more dominant. This could be an explanation for the experimentally obtained trend of the melt viscosity that features a maximum for $Cu_{50}Ti_{50}$ as will be seen below. There, the high affinity of Cu-Ti and a higher number of Cu-Ti pairs as compared to $Cu_{76}Ti_{24}$ apparently lead to a significant slowdown of the viscosity, as was experimentally observed [21].

B. Coordination numbers

The coordination number distributions are determined by counting the number of neighboring Cu and Ti atoms within the first coordination shell defined by the first minimum of the corresponding partial pair-correlation functions $g_{\alpha\beta}(r)$. They are plotted for both Cu and Ti in the liquid (1700 K) and undercooled region (1000 K) in Fig. 4. They give a first indication of the nature of the SRO. Upon cooling, we observe an increase in the coordination numbers for both Cu and Ti. Similar results have also been obtained by using the Radical Voronoi Tessellation method. This is in contrast to, e.g., the Cu-Zr system, where the opposite behavior has been found [14]. In both, the liquid and undercooled region, Cu features mainly a Z12 coordination, i.e., a large fraction of the Cu atoms are surrounded by a simple icosahedron, as will become clearer from the CNA discussion below. This also agrees with the calculated ratios of the respective peak positions of the total structure factor $S(q)$ listed in Table II, which already indicated the presence of an ISRO. An ISRO is not compatible with a long-range periodicity of the crystalline phase and might already explain the large degree of undercooling of the Cu-Ti system and thus the potentially good GFA of Cu-Ti-based alloys [44].

C. Common neighbor analysis

By performing a CNA on inherent configurations of the melt, an even more detailed image of the topology of the polyhedra surrounding the Cu and Ti atoms is obtained.

The most important bonded pairs for all compositions in the undercooled and liquid state (1000 K and 1700 K) are reported in Table III. The numbers within the square brackets represent specific structural characteristics of atomic clusters. After identifying all neighboring atoms with a specified cutoff radius R_c corresponding to the first minimum of the partial pair-correlation function around a selected atom, each pair formed by the atom and its neighbors is analyzed. The goal is to characterize the common neighbors of each pair in the first coordination shell using a set of three indices jkl: j represents the number of neighbors shared by both atoms, k denotes the number of bonds between these shared neighbors (a bond is considered present if the distance between neighbors is smaller than R_c), and l indicates the number of bonds in the longest chain among the common neighbors. Before discussing the found cluster symmetries, it is worth highlighting the absence or negligible amounts of [421] and [422] symmetries, which would signal the presence of a fcc and hcp ordering like in solid Cu and Ti, respectively. Thus, it is assured that a fully liquid system is present during our simulations. In contrast, an underlying bcc structure, which is indicated by the small, but non-negligible amount of [444] symmetry, cannot be fully excluded when associated to [666] pairs.

TABLE III. Common-neighbor analysis for $Cu_{31}Ti_{69}$, $Cu_{50}Ti_{50}$, and $Cu_{76}Ti_{24}$ at $T = 1000$ K and 1700 K (undercooled and stable liquid region). The error bars for the calculated pair abundances are of the order of 0.01. Please note that the given values for [666] also include the fraction of the distorted sixfold symmetry [677].

	$Cu_{31}Ti_{69}$				$Cu_{50}Ti_{50}$				$Cu_{76}Ti_{24}$			
	Cu		Ti		Cu		Ti		Cu		Ti	
CNA (%)	1000 K	1700 K	1000 K	1700 K	1000 K	1700 K	1000 K	1700 K	1000 K	1700 K	1000 K	1700 K
[421]	0.00	1.72	0.00	1.44	1.14	2.23	0.00	1.97	1.18	2.79	0.00	1.89
[422]	1.86	4.53	1.89	3.57	2.30	4.35	1.71	3.26	1.95	5.31	1.71	4.43
[433]	14.4	18.2	11.7	14.8	14.4	19.0	9.79	15.2	14.7	19.2	10.6	15.9
[444]	9.34	8.91	7.36	7.19	8.72	7.71	7.16	7.00	9.70	7.23	8.28	6.27
[544]	12.6	14.4	14.8	15.2	13.8	13.7	14.7	14.8	12.6	14.7	14.0	16.7
[555]	40.4	19.1	26.5	21.3	37.2	18.1	35.0	19.0	34.2	17.5	31.2	19.1
[666]	11.3	9.72	18.1	13.9	12.3	9.76	19.9	14.2	12.7	9.24	18.2	13.8

In general, upon undercooling, an increase for all pairs, except for the [433] one, is observed, indicating an increasing order of the melt. This agrees with the coordination number, which also, on average, increase for both Cu and Ti upon cooling. In general, a FFS i.e., an ISRO, which is represented by the [555] pairs and its distorted version [554], is already present in the liquid state for both Cu and Ti, while upon undercooling, a strong increase, especially for Cu is observed. With the high fraction of Z12 coordination for Cu, the strong occurrence of the [555] symmetry, especially in the undercooled melt, is also a strong indicator for the good undercooling rate and potentially high GFA of the Cu-Ti and its multicomponent systems.

Associated to [555], the CNA reveals a significant amount of [666] symmetry, essentially around Ti. This refers to high coordination polyhedra, most likely Frank-Kasper polyhedra. Upon cooling, this [666] symmetry increases especially for Ti, which is in good agreement with the high coordination numbers found for Ti. In addition, a smaller, but non-negligible amount of [444] is found, highlighting a competition between the Frank-Kasper and bcc ordering. The only type of symmetry that is decreasing upon cooling is the [433] ordering, which can be seen as distorted pair with a five- or fourfold symmetry, thus indicating that the liquid becomes more structured. For all compositions, the fivefold [555] symmetry increases the strongest upon decreasing temperature, and thus we can conclude that the [433] ordering in the melt transforms mainly into a [555] symmetry around Cu, while a significantly smaller fraction transforms into a [444] ordering, typical of the bcc ordering. Overall, $Cu_{50}Ti_{50}$ features the highest amount of a fivefold and [666] symmetry. In addition, upon undercooling the melt, the amount of [433] pairs decreases the strongest for $Cu_{50}Ti_{50}$. Consequently, the FFS symmetry of $Cu_{50}Ti_{50}$ increases the strongest upon cooling. The detailed structural picture can be used to explain the melt dynamics, which are the slowest for $Cu_{50}Ti_{50}$. While an ISRO is known to slow down melt dynamics [40], the complex coordination scenario, especially around Ti, contributes as well: Atom diffusion would affect many atoms coordinated in Frank-Kasper polyhedra around the center atom (Z15 and Z16) and is therefore not favored, which in turn slows down the melt dynamics. The fact that $Cu_{50}Ti_{50}$ exhibits the slowest melt dynamics as well as the highest FK polyhedra fraction (see Table III) underlines this assumption.

In the undercooled melt, with decreasing Ti content, the fraction of Z12 coordination slightly decreases, whereas a Z13 coordination, meaning a distorted fivefold ISRO, becomes more dominant for Cu. Over the entire temperature range, the coordination numbers for Ti are significantly higher than for Cu, suggesting a more complex coordination polyhedron than the simple icosahedron. We observe a non-negligible amount of Z15 and Z16 coordination for Ti, which can be addressed to Frank-Kasper polyhedra due to the presence of [666] pairs. For Cu, we also observe higher coordination numbers (Z13 and Z14), however, to a significant lower degree. Thus, the complexity of the coordination scenario around Ti is apparently higher than for Cu. This applies, in particular, for $Cu_{76}Ti_{24}$, where the fractions of Z15 and Z16 coordination is the highest. By taking into account the strong amplitude of the first peak of g_{CuTi}, which indicates the preferential presence of heterogeneous Cu-Ti pairs, the high coordination numbers around Ti can also explain the increasing Ti-Ti distances with decreasing Ti-content [cf. Fig. 3(f)]. With more Ti atoms that are preferably surrounded by Cu atoms, the average Ti-Ti distance increases. The weak amplitude of the first maxima of g_{TiTi}, especially for $Cu_{76}Ti_{24}$, confirms this assumption.

In summary, CNA allows us to extract a detailed three-dimensional picture about the short-range order and its evolution upon decreasing temperature. Generally, the way in which the SRO evolves upon undercooling is similar for all investigated Cu-Ti alloys. The FFS is found to be the most important feature: For Cu, the FFS increases linearly with increasing Cu content, while around Ti the FFS is the highest at intermediate Ti contents. In total, the FFS fraction is highest for $Cu_{50}Ti_{50}$, which provides an explanation for the slowest melt dynamics, which was found for this composition. High coordination Frank-Kasper polyhedra are present, in particular, around Ti, and an underlying bcc ordering is obtained as well, suggesting a competition between the FFS and the bcc orderings [45]. Interestingly, the [666] fraction is the highest for an intermediate Ti content, and leads to the assumption that these Frank-Kasper polyhedra also contribute to the slowdown of the Cu-Ti system.

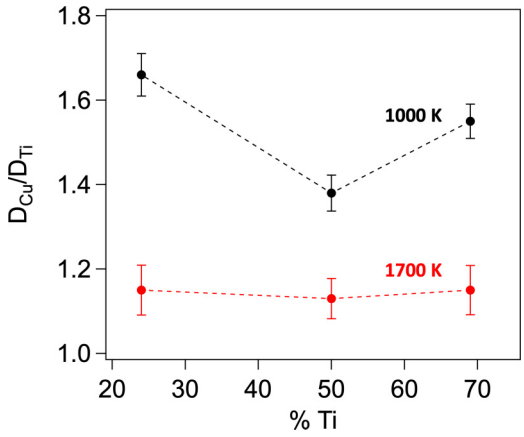

FIG. 5. Ratio D_{Cu}/D_{Ti} from AIMD simulations, depending on the composition at 1000 K (black) and 1700 K (red). The dashed lines are guides to the eye.

D. Dynamic properties of Cu-Ti alloys

Figure 5 shows the ratio of Cu and Ti diffusion coefficients D_{Cu}/D_{Ti} as a function of Ti content, calculated with AIMD simulations at 1000 K and 1700 K. Thereby, the dynamical decoupling of the atomic species and its dependence on the composition can be addressed, which is not possible experimentally. Please note that only the longer timescales of the AIMD simulations (from 12 ps), in which the atoms are in a purely diffusive state, namely, a well-established linear regime, were considered for the extraction of the diffusion coefficients. At high temperatures (1700 K), the D_{Cu}/D_{Ti} ratio remains constant around a value of 1.15 over the entire composition range. The situation changes when decreasing the temperature. At 1000 K significantly higher values of the D_{Cu}/D_{Ti} ratio for all Cu-Ti compositions are obtained, suggesting an overall decoupling of the diffusion coefficients. In particular, the high values at the Ti-rich side, indicate weak Cu-Ti interactions: the smaller Cu atoms are weakly bound to the larger Ti atoms, and can move more readily through the melt, thereby leading to the decoupling of the diffusion coefficients. This is in contrast to other systems, e.g., binary Ni-Zr, where stronger interactions between Ni and Zr and no decoupling at the Ni-rich side have been found [20,46]. Here, with increasing Ti content, the D_{Cu}/D_{Ti} ratio first decreases from 1.66 ± 0.04 to 1.38 ± 0.04 for $Cu_{50}Ti_{50}$ before increasing to 1.55 ± 0.05 for $Cu_{31}Ti_{69}$. This observed composition dependency results from the changing numbers of Cu-Ti pairs, which is the highest for the equiatomic $Cu_{50}Ti_{50}$ composition, where also the strongest D_{Cu}/D_{Ti} is found. As a consequence of this, a large fraction of FFS and complex Frank-Kasper polyhedra forms. In other words, the melt dynamics are governed by the local structure, which is a consequence of the present chemical interactions, which show a pronounced composition dependence at a low temperature of 1000 K.

In addition to the diffusion coefficients, the effect of the local structure and the present symmetry on the dynamic properties of stable and undercooled liquids can be investigated by calculating the respective viscosities. Figure 6 shows the calculated viscosity as a function of Ti content for the stable and undercooled liquid at 1300 K and 1000 K,

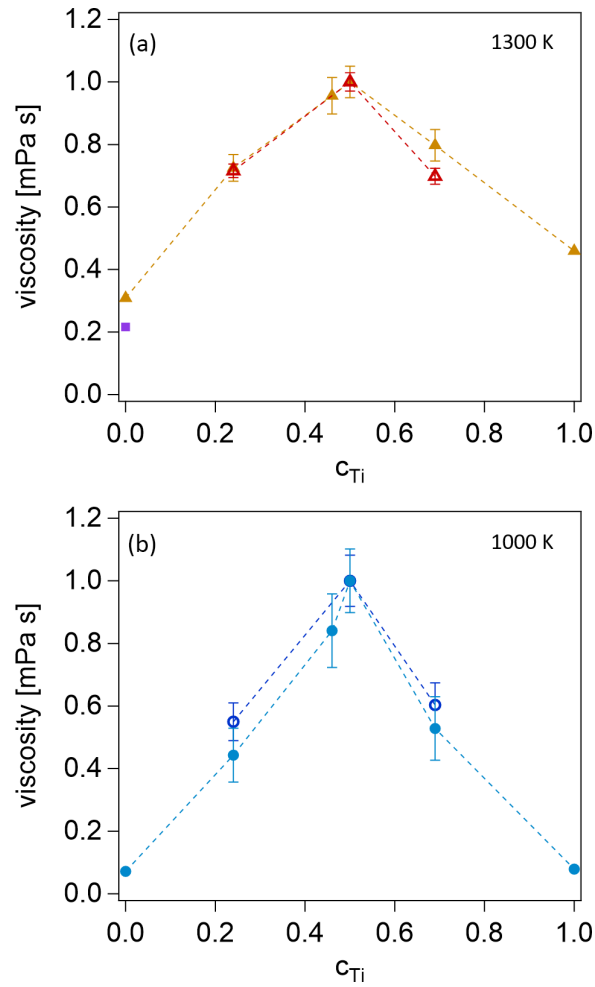

FIG. 6. Evolution of the calculated viscosity in the (a) liquid and (b) undercooled region at 1300 K (open orange triangles) and 1000 K (open blue circles), respectively, as a function of the Ti content, including error bars of 15%. The values have been normalized to the respective highest viscosity. Experimental data are shown as full symbols according to Ref. [21], whereas the temperature slightly differs from those of the calculated viscosities ($T = 1030$ and 1273 K). The data for pure Cu and liquid has been extrapolated from experimental data that was available within a temperature range of 1360 to 1960 K for Cu and 1730 to 2120 for Ti [48–50]. The viscosity of pure Cu at a temperature of approximately 1380 K, computed by a direct method using the transverse current-current correlation function $C_T(q,t)$, is shown as full purple square and was taken from Ref. [24].

respectively. The viscosity has been calculated according to the Stokes-Einstein (SE) relation $\eta_E = k_B T/2\pi RD$, where k_B is Boltzmann's constant and R the average interatomic particle distance at temperature T. Furthermore, D stands for the mean self-diffusion coefficient. The calculated values are compared to the experimentally obtained viscosities, which are also plotted in Fig. 6 (closed symbols). Please note that the respective temperatures amount to 1273 K and 1030 K, and thus differ slightly from the temperatures of the calculated values, which are 1300 K and 1000 K.

In general, the calculated values using the SE relation are lower than the experimentally measured ones. This refers to

the breakdown of the SE relation: Upon alloying pure Cu and Ti, local structures evolve around the respective species as has been shown above. The familiar SE relation, which uses the effective radii from partial pair-correlation functions, is not capable of taking these local structures into account and instead assumes a uniform diffusion of both Cu and Ti atoms. Thus, the SE relation is oversimplified and not valid, in general, for binary or multicomponent alloys. However, a constant error is obtained with respect to the composition, which means that the obtained compositional trend is qualitatively correct. To allow for better comparison between the experimental and calculated values, we normalize all values to the highest viscosity. At both temperatures, 1000 K and 1300 K, the AIMD simulations are able to reproduce the viscosity maximum at intermediate Ti contents. This further indicates a correct representation of the Cu-Ti correlation, as well as the local structures and coordination scenarios around Cu and Ti. In addition, the normalized viscosity of pure Cu at a temperature of approximately 1380 K is plotted in Fig. 6(a) (full purple square). This value was calculated by a direct method using the transverse current-current correlation function $C_T(q,t)$ as described in Refs. [24,47]. It has been shown that this approach leads to reliable values of the shear viscosity for metallic liquids with an error bar on the order of 0.2 mPa s. In the case of pure Cu, the computed value (≈4 mPa s) is reasonably close to the experimentally found value (≈6 mPa s), especially when considering that the calculated value has been derived at a higher temperature of 1380 K as compared to 1273 K for the experimental viscosity. Especially in the undercooled regime at 1000 K, the viscosity of the equiatomic $Cu_{50}Ti_{50}$ composition was found to be the highest, which can be explained by the highest FFS fraction and complex coordination scenario, reflected by the high fraction of Frank-Kasper polyhedra. From AIMD, the $Cu_{50}Ti_{50}$ was found to exhibit the highest fraction of FFS (around Cu and Ti) and thus might be responsible for the increased melt viscosity. Furthermore, a maximum of the high coordination Frank-Kasper polyhedra was also found for $Cu_{50}Ti_{50}$, which further promotes an increased viscosity. This is also consistent with the strongest Cu-Ti correlation of $Cu_{50}Ti_{50}$ found via the D_{Cu}/D_{Ti} ratio (cf. Fig. 5).

IV. CONCLUSION

First-principles based AIMD simulations have been performed for binary Cu_xTi_{1-x} ($x = 0.31$, 0.50, and 0.76) alloys over a wide temperature range, covering both liquid and undercooled states, to investigate the relationship of the local structure and dynamical properties. The CNA reveals increasing local order with decreasing temperature, dominated by a FFS around Cu. Especially in the undercooled region, higher coordination numbers that are compatible with Frank-Kasper polyhedra were obtained for Ti and to a lower degree also for Cu. In addition, the FFS and Frank-Kasper polyhedra compete with a bcc ordering. The found local structure results from weak Cu-Ti interactions, while it is also dependent on the alloy composition, i.e., the number of Cu-Ti bonds. A maximum of FFS is found for the equiatomic $Cu_{50}Ti_{50}$ composition. Also, the fraction of Frank-Kasper polyhedra around Ti is the highest. These local structures lead to strong Cu-Ti correlations and a maximum in the melt viscosity, which was found experimentally and via AIMD simulations. This correlation suggests that the melt viscosity is mainly slowed down by the FFS symmetry and the complexity of the local structure and coordination scenario, whereas attractive chemical interactions between Cu and Ti, i.e., the preferred formation of Cu-Ti pairs, seem to play a subordinate role. Instead, a behavior close to an ideal-solution behavior was found, which agrees with recent experimental studies. With the use of *ab initio* simulations, the focus of this paper was on local ordering and dynamical effects. To study long-range effects as well, another approach could be used, which includes the development of machine learning interatomic potentials that are trained on appropriate sets of AIMD configurations. This allows us to perform million-atom molecular dynamics simulations with the accuracy close to *ab initio* [51,52].

ACKNOWLEDGMENTS

We thank Prof. W. Petry for constructive discussions of the experimental Cu-Ti data and Dr. Alaa Fahs for technical help with the AIMD simulations. Financial support provided by the Deutsche Forschungsgemeinschaft (DFG) via Grants No. PE580/20-4 and No. YA418/1-4 is gratefully acknowledged. Furthermore, we acknowledge the CINES, IDRIS, and TGCC under Project No. INP2227/72914/gen5054, as well as CIMENT/GRICAD for computational resources. We acknowledge financial support under the French-German project PRCI ANR-DFG SOLIMAT (ANR-22-CE92-0079-01). This work has been partially supported by MIAI@Grenoble Alpes (ANR-19-P3IA-0003). Discussions within the French collaborative network in artificial intelligence in materials science GDR CNRS 2123 (IAMAT) are also acknowledged.

[1] D. Xu, B. Lohwongwatana, G. Duan, W. L. Johnson, and C. Garland, Bulk metallic glass formation in binary Cu-rich alloy series – $Cu_{100-x}Zr_x$ ($x = 34$, 36, 38.2, 40 at.%) and mechanical properties of bulk $Cu_{64}Zr_{36}$ glass, Acta Mater. **52**, 2621 (2004).

[2] D. Wang, Y. Li, B. B. Sun, M. L. Sui, K. Lu, and E. Ma, Bulk metallic glass formation in the binary Cu–Zr system, Appl. Phys. Lett. **84**, 4029 (2004).

[3] L. Xia, D. Ding, S. T. Shan, and Y. D. Dong, The glass forming ability of Cu-rich Cu-Hf binary alloys, J. Phys.: Condens. Matter **18**, 3543 (2006).

[4] L. Xia, W. H. Li, S. S. Fang, B. C. Wei, and Y. D. Dong, Binary Ni–Nb bulk metallic glasses, J. Appl. Phys. **99**, 026103 (2006).

[5] D. B. Miracle, D. V. Louzguine-Luzgin, L. V. Louzguina-Luzgina, and A. Inoue, An assessment of binary metallic glasses: Correlations between structure, glass forming ability and stability, Inter. Mater. Rev. **55**, 218 (2010).

[6] T. Zhang, K. Kurosaka, and A. Inoue, Thermal and mechanical properties of Cu-based Cu-Zr-Ti-Y bulk glassy alloys, Mater. Trans. **42**, 2042 (2001).

[7] D.-M. Lee, J.-H. Sun, S.-Y. Shin, J.-C. Bae, and C.-H. Lee, Improvement of glass forming ability of Cu-Ni-Zr-Ti alloys by substitution of Hf and Nb, Mater. Trans. **49**, 1486 (2008).

[8] X. Wu, Z. Suo, Y. Si, L. Meng, and K. Qiu, Bulk metallic glass formation in a ternary Ti-Cu-Ni alloy system, J. Alloys Compd. **452**, 268 (2008).

[9] S. Amore, J. Brillo, I. Egry, and R. Novakovic, Surface tension of liquid Cu-Ti binary alloys measured by electromagnetic levitation and thermodynamic modelling, Appl. Surf. Sci. **257**, 7739 (2011).

[10] P. Gargarella, S. Pauly, M. de Oliveira, U. Kühn, and J. Eckert, Glass formation in the Ti-Cu system with and without Si additions, J. Alloys Compd. **618**, 413 (2015).

[11] B. Shang, N. Jakse, P. Guan, W. Wang, and J. l. Barrat, Influence of oscillatory shear on nucleation in metallic glasses: A molecular dynamics study, Acta Mater. **246**, 118668 (2023).

[12] S. Cao, M. Xia, N. Jakse, L. Zeng, P. Yu, Y. Zhao, W. Lu, and J. Li, Influence of Zr element on the atomic structure of Al-Cu alloy liquid, Scr. Mater. **248**, 116143 (2024).

[13] T. Mei-Bo, Z. De-Qian, P. Ming-Xiang, and W. Wei-Hua, Binary Cu-Zr bulk metallic glasses, Chin. Phys. Lett. **21**, 901 (2004).

[14] N. Jakse and A. Pasturel, Local order and dynamic properties of liquid and undercooled Cu_xZr_{1-x} alloys by *ab initio* molecular dynamics, Phys. Rev. B **78**, 214204 (2008).

[15] F. Yang, D. Holland-Moritz, J. Gegner, P. Heintzmann, F. Kargl, C. C. Yuan, G. G. Simeoni, and A. Meyer, Atomic dynamics in binary Zr-Cu liquids, Europhys. Lett. **107**, 46001 (2014).

[16] N. Jakse, T. L. T. Nguyen, and A. Pasturel, Local order and dynamic properties of liquid and undercooled $Cu_{55}Hf_{45}$ and $Cu_{62}Hf_{38}$ alloys by *ab initio* molecular dynamics, J. Appl. Phys. **114**, 063514 (2013).

[17] D. Holland-Moritz, S. Stüber, H. Hartmann, T. Unruh, T. Hansen, and A. Meyer, Structure and dynamics of liquid $Ni_{36}Zr_{64}$ studied by neutron scattering, Phys. Rev. B **79**, 064204 (2009).

[18] D. Herlach, P. Galenko, and D. Holland-Moritz, *Metastable Solids from Undercooled Melts* (Elsevier, Burlington, MA, 2007).

[19] D. Holland-Moritz, F. Yang, T. Kordel, S. Klein, F. Kargl, J. Gegner, T. Hansen, J. Bednarcik, I. Kaban, O. Shuleshova, N. Mattern, and A. Meyer, Does an icosahedral short-range order prevail in glass-forming Zr-Cu melts? Europhys. Lett. **100**, 56002 (2012).

[20] B. Nowak, D. Holland-Moritz, F. Yang, T. Voigtmann, Z. Evenson, T. C. Hansen, and A. Meyer, Effect of component substitution on the atomic dynamics in glass-forming binary metallic melts, Phys. Rev. B **96**, 054201 (2017).

[21] L. P. Kreuzer, F. Yang, Z. Evenson, D. Holland-Moritz, A. Bernasconi, T. C. Hansen, M. Blankenburg, A. Meyer, and W. Petry, Dynamical and structural properties of undercooled Cu-Ti melts investigated by neutron and x-ray diffraction, Phys. Rev. B **109**, 174108 (2024).

[22] N. Jakse and A. Pasturel, Glass forming ability and short-range order in a binary bulk metallic glass by *ab initio* molecular dynamics, Appl. Phys. Lett. **93**, 113104 (2008).

[23] C. Woodward, M. Asta, D. R. Trinkle, J. Lill, and S. Angioletti-Uberti, *Ab initio* simulations of molten Ni alloys, J. Appl. Phys. **107**, 113522 (2010).

[24] N. Jakse and A. Pasturel, Relationship between structural and dynamic properties of Al-rich Al-Cu melts: Beyond the Stokes-Einstein relation, Phys. Rev. B **94**, 224201 (2016).

[25] A. Pasturel and N. Jakse, Stokes-Einstein relation and excess entropy in Al-rich Al-Cu melts, Appl. Phys. Lett. **109**, 041904 (2016).

[26] J. Li, R. Xiao, J. Qin, Y. Ruan, and H. Li, The structural exploration of thermodynamics and dynamics in Ti-Ni liquid by *ab initio* molecular dynamics simulation, Comput. Mater. Sci. **230**, 112499 (2023).

[27] G. Kresse and J. Hafner, *Ab initio* molecular dynamics for liquid metals, Phys. Rev. B **47**, 558 (1993).

[28] P. E. Blöchl, Projector augmented-wave method, Phys. Rev. B **50**, 17953 (1994).

[29] G. Kresse and D. Joubert, From ultrasoft pseudopotentials to the projector augmented-wave method, Phys. Rev. B **59**, 1758 (1999).

[30] J. P. Perdew and A. Zunger, Self-interaction correction to density-functional approximations for many-electron systems, Phys. Rev. B **23**, 5048 (1981).

[31] S. Nosé, A unified formulation of the constant temperature molecular dynamics methods, J. Chem. Phys. **81**, 511 (1984).

[32] K. Binder and W. Kob, *Glassy Materials and Disordered Solids*, revised ed. (World Scientific, Singapore, 2011).

[33] F. H. Stillinger and T. A. Weber, Hidden structure in liquids, Phys. Rev. A **25**, 978 (1982).

[34] D. Faken and H. Jónsson, Systematic analysis of local atomic structure combined with 3D computer graphics, Comput. Mater. Sci. **2**, 279 (1994).

[35] A. Stukowski, Visualization and analysis of atomistic simulation data with OVITO–the Open Visualization Tool, Modell. Simul. Mater. Sci. Eng. **18**, 015012 (2010).

[36] D. Holland-Moritz, F. Yang, T. Hansen, and F. Kargl, Chemical short-range order in liquid Ni-Cu, J. Phys.: Condens. Matter **35**, 465403 (2023).

[37] D. Holland-Moritz, O. Heinen, R. Bellissent, and T. Schenk, Short-range order of stable and undercooled liquid titanium, Mater. Sci. Eng. A **449-451**, 42 (2007).

[38] S. Sachdev and D. R. Nelson, Theory of the structure factor of metallic glasses, Phys. Rev. Lett. **53**, 1947 (1984).

[39] E. Sondermann, N. Jakse, K. Binder, A. Mielke, D. Heuskin, F. Kargl, and A. Meyer, Concentration dependence of interdiffusion in aluminum-rich Al-Cu melts, Phys. Rev. B **99**, 024204 (2019).

[40] T. Schenk, D. Holland-Moritz, V. Simonet, R. Bellissent, and D. M. Herlach, Icosahedral short-range order in deeply undercooled metallic melts, Phys. Rev. Lett. **89**, 075507 (2002).

[41] J. P. Hansen and I. R. McDonald, *The Theory of Simple Liquids*, 3rd ed. (Academic Press, Oxford, 2006).

[42] S. Amore, J. Horbach, and I. Egry, Is there a relation between excess volume and miscibility in binary liquid mixtures? J. Chem. Phys. **134**, 044515 (2011).

[43] S. Amore, S. Delsante, H. Kobatake, and J. Brillo, Excess volume and heat of mixing in Cu-Ti liquid mixture, J. Chem. Phys. **139**, 064504 (2013).

[44] F. C. Frank and N. F. Mott, Supercooling of liquids, Proc. R. Soc. London A **215**, 43 (1952).

[45] N. Jakse and A. Pasturel, Local order of liquid and supercooled zirconium by *ab initio* molecular dynamics, Phys. Rev. Lett. **91**, 195501 (2003).

[46] S. W. Basuki, F. Yang, E. Gill, K. Rätzke, A. Meyer, and F. Faupel, Atomic dynamics in Zr-based glass forming alloys near the liquidus temperature, Phys. Rev. B **95**, 024301 (2017).

[47] N. Jakse and A. Pasturel, Liquid aluminum: Atomic diffusion and viscosity from *ab initio* molecular dynamics, Sci. Rep. **3**, 3135 (2013).

[48] M. J. Assael, A. E. Kalyva, K. D. Antoniadis, R. M. Banish, I. Egry, J. Wu, E. Kaschnitz, and W. A. Wakeham, Reference data for the density and viscosity of liquid copper and liquid tin, J. Phys. Chem. Ref. Data **39**, 033105 (2010).

[49] P.-F. Paradis, T. Ishikawa, and S. Yoda, Non-contact measurements of surface tension and viscosity of niobium, zirconium, and titanium using an electrostatic levitation furnace, Int. J. Thermophys. **23**, 825 (2002).

[50] T. Ishikawa, P.-F. Paradis, J. T. Okada, and Y. Watanabe, Viscosity measurements of molten refractory metals using an electrostatic levitator, Meas. Sci. Technol. **23**, 025305 (2012).

[51] J. Behler, Four generations of high-dimensional neural network potentials, Chem. Rev. **121**, 10037 (2021).

[52] N. Jakse, J. Sandberg, L. F. Granz, A. Saliou, P. Jarry, E. Devijver, T. Voigtmann, J. Horbach, and A. Meyer, Machine learning interatomic potentials for aluminium: Application to solidification phenomena, J. Phys.: Condens. Matter **35**, 035402 (2023).